Ceramics-Silikáty 63 (4), 449-459 (2019)
www.ceramics-silikaty.cz doi: 10.13168/cs.2019.0041

MULTI-INSTRUMENTAL CHARACTERISATION OF DECORATIVE LAYERS IN GLAZED CERAMIC RELIEFS FROM THE SCHWARZENBERG PALACE IN PRAGUE

#ALEXANDRA KLOUŽKOVÁ*, RADKA ŠEFCŮ**, IVANA TURKOVÁ***, MÁRIA KOLÁŘOVÁ*
MARTINA BAJEUX KMONÍČKOVÁ**, PAVLA DVOŘÁKOVÁ*

*Department of Glass and Ceramics, University of Chemistry and Technology, Prague,
Technická 5, 166 28 Prague, Czech Republic
**Chemical-Technological Laboratory, National Gallery Prague, Staroměstské nám. 12, 110 15 Prague, Czech Republic
***Department of Microscopy, Institute of Criminalistics, Bartolomějská 12, 110 00 Prague, Czech Republic

#E-mail: klouzkoa@vscht.cz

Submitted June 24, 2019; accepted August 23, 2019

Keywords: Glazes, Ceramics, Raman spectroscopy, Scanning electron microscopy, Pigments, Dyes, Cultural heritage, Archaeology, Naples yellow

This paper presents recent research results on glazes and ceramic bodies in glazed ceramic lunette reliefs from the second half of the 16th century. The main objective was to identify dyes in the coloured coatings and defects in the glazes using multiple instrumental techniques (X-ray fluorescence, portable X-ray fluorescence, X-ray diffraction, micro-Raman spectroscopy, scanning electron microscopy and elemental SEM-EDS analysis, dilatometry and thermomechanical analysis). The research confirmed the presence of ionic dyes (Cu, Fe, Co, Sb, Mn ions) in medium lead glazes (approx. 28 – 63 wt. %), but also various types of yellow pigments in the Pb–Sb, Pb–Sn and the Pb–Sb–Sn systems were identified. Various defects were observed on the surface of glazes. In the case of the yellow glaze, the examination showed a lower lead content in the top layer. The defects – corrosion holes – were caused by selective corrosion in the environment of the waste pit. The green glazes in the lunette reliefs were damaged due to ageing of ceramics fired at low temperatures or due to irreversible moisture expansion of ceramic bodies.

INTRODUCTION

Archaeological research in the Schwarzenberg Palace [1-2] uncovered two large-format lunette reliefs with a plastic decoration featuring the Czech lion inside a shield surrounded by a vegetal motif (Figure 1). Although the same mould was used to make the lunettes, the surface finish is different in each of them. The first relief is glazed with a monochrome green glaze (first half of the 16th century, Schwarzenberg Palace, Prague 1, Institute of Archaeology of the CAS, Prague, v. v. i., id. no. 614), while the second lunette relief features colourful glazes with additional polychrome layers (first half of the 16th century, Schwarzenberg Palace, Prague 1, Institute of Archaeology of the CAS, Prague, v. v. i., id. no. 886).

During the material investigation conducted prior to the restoration process, surface polychrome layers and secondary layers were analyzed using selected fragments from both of the lunette reliefs (Figure 2).

The study aimed primarily at the characterisation of glazes, pigments and ceramic bodies. Based on the results of these analyses, we subsequently focused on verifying the assumption that both reliefs were made in the same workshop. For this reason, we compared the green glazes (composition of the main glassy phase and identification of colouring agents) and ceramic bodies (composition of the matrix, determination of temper and admixtures) in both of the reliefs. In another part of the research, we aimed at the identifying the origin and source of glaze defects observed in some of the fragments. The defects largely included crazing and peeling of the basic green glaze (Figure 3). Some types of glaze defects occur immediately after the ceramic product is fired, while other types appear during utilization of the product. Moreover, in the case of archaeological finds, defects may occur due to unsuitable environmental conditions (especially relative humidity and temperature).

Non-invasive and non-destructive analytical methods such as portable X-ray fluorescence analysis (p-XRF), micro-Raman spectroscopy (MRS) and solid-sample analysis of compact flat decorated surfaces (XRF, XRD) are of course the preferable options in research focusing on identifying and characterising materials in cultural heritage objects [3-6]. Analytical methods that require using micro-samples, such as scanning electron microscopy (SEM), present another option. When thermal analysis, especially dilatometry (DIL), is applied to identify the causes of degradation, it

a) green lunette A (no. 614)

b) multi-colour lunette B (no. 886)

Figure 1. Large-format lunette reliefs after restoration: a) green lunette A (no. 614), b) multi-colour lunette B (no. 886) , foto L. Svobodova..

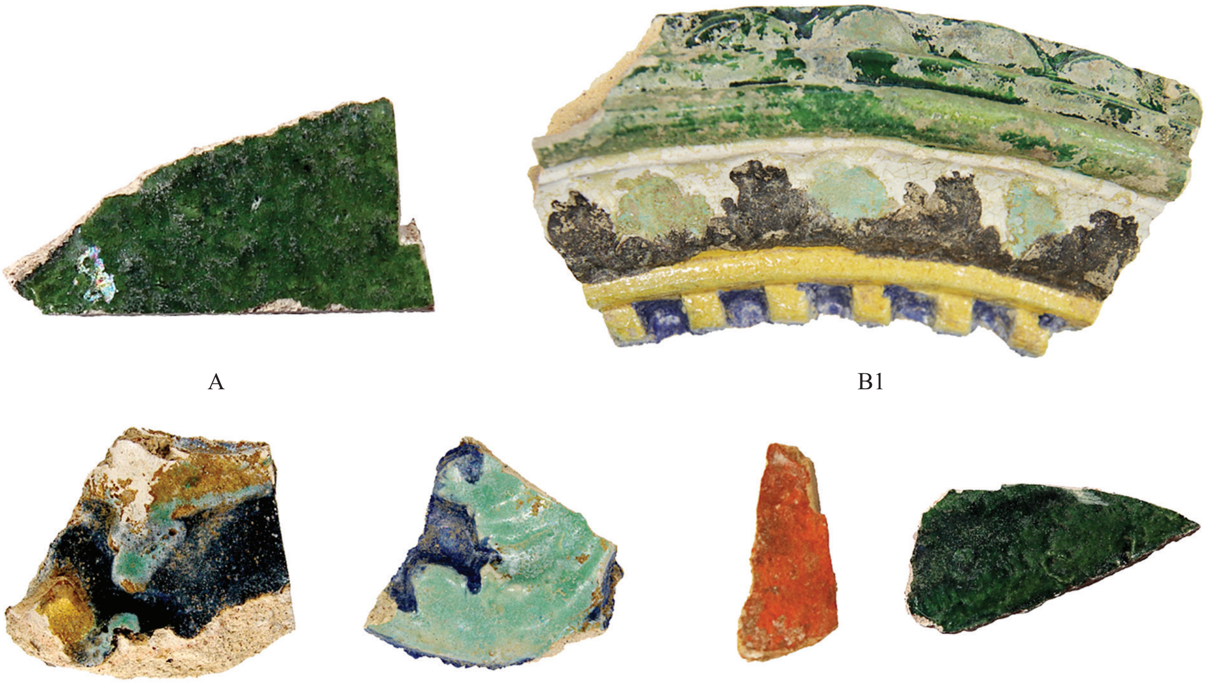

A

B1

B2

B3

B4

B5

Figure 2. Fragments of reliefs: A – green lunette, B1 – multi-colour lunette fragment 1, B2 – multi-colour lunette fragment 2, B3 – multi-colour lunette fragment 3, B4 – multi-colour lunette fragment 4, B5 – multi-colour lunette fragment 5.

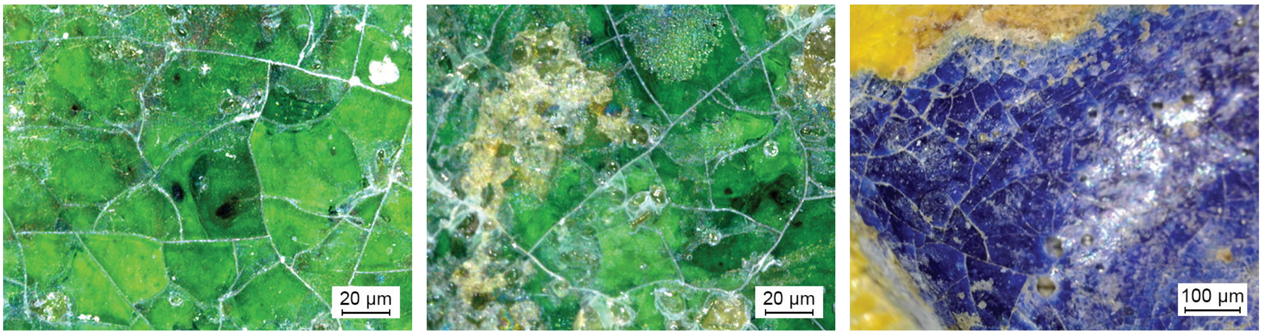

A

B5

B1

Figure 3. Surface defects in green glazes: A – green lunette, B – multi-colour lunette fragment B5 and B2.

is necessary to prepare a larger, compact sample (regular prism approx. 20 mm long) from a suitable place on the fragment (here, we used the lower part of the green lunette relief). The wide range of analytical techniques used for the examination of artworks allow us to gather sufficient complementary results for identifying the material used (i.e. colouring agents, tempers etc.), determining the manufacturing process (i.e. the way surface coating was applied, sources of raw materials etc.) and detecting degradation processes.

EXPERIMENTAL

At first, non-invasive analyses were performed and micro-samples were taken (Table 1) from both green (fragment A, Figure 2) and multi-colour relief lunettes (fragments B1-B5, Figure 2).

Sample preparation

10 micro-samples were taken during the investigation of glazes and ceramic bodies. 9 of these samples were taken from the multi-colour relief lunette and 1 from the green relief lunette. Micro-samples of the glazes and polychrome were fixed in methyl-methacrylate resin (ClaroCit, Struers). After hardening, the cross-sections were gradually dry-ground and polished with the silicium carbide SiC abrasive material to allow for transversal observation and analysis of the different layers.

Non-invasive documentation methods

Macro-photographic documentation was performed using a USB microscope Dino-Lite Pro AM4113ZT-FV2W, polarised and ultraviolet light (λ = 375 nm), 1.3 megapixel, magnification 50×, 200×. The photographs were processed in the program DinoCapture 2.0 and NIS Elements D.

Analysis methods

Non-invasive chemical analyses were used as the first step in the investigation. Chemical compositions were analysed using a hand-held portable XRF spectro-meter NITON XL3t GOLDD+ (Thermo Scientific). This instrument is equipped with an Ag tube and operates at the voltage of 50 kV and the current of 50 µA. For light elements, we used the voltage of 8 kV and the current of 200 µA. The measurement is able to detect elements from Al to U. Induced radiation in the sample was detected using an integrated large-area silicon drift detector. The working distance was approx. 1 mm with the beam diameter under 4 mm and the acquisition time 120 s. As the second step, we conducted powder X-ray fluorescence analysis. The chemical composition of finely powdered ceramic bodies were determined using an ARL 9400 XP sequential WD-XRF spectrometer equipped with a Rh anode end-window X-ray tube type 4GN fitted with 50-lm Be window. The generator settings – collimator – crystal – detector combinations were optimized for all 82 measured elements with analysis time 6 s per element. The data obtained from these measurements were evaluated using standardless software Uniquant 4 [4].

Mineralogical analyses (XRD) of both the fine powders from ceramic bodies and the compact samples of glazes were carried out using an X'Pert PRO θ–θ powder diffractometer with parafocusing Bragg–Brentano geometry and CuKα radiation (λ = 1.5418 nm, U = 40 kV, I = 30 mA) at the room temperature. The data were evaluated using the software package HighScore Plus 3.0e .

Cross-sections were studied using an Eclipse 600 Nikon polarising microscope (PLM) in visible light and in dark field, and after excitation by UV light using an Hg discharge lamp and UV filter with a wavelength range 330 – 380 nm and 450 – 490 nm. The usual magnification was 200 – 500 ×. Micrographs of the cross-sections from actual samples were taken using a DS-Fi2 Nikon digital camera.

Table 1. Description of the samples from the ceramic body, the glazes and polychromy, and analyses included in this study.

Position and color glazes	p-XRF	XRF	PLM	MRS	SEM-EDS	XRD
Green lunette A						
dark green A	+	+	+	+	+	+
ceramic body A	+	+	+	+	+	+
Multi-color lunette B						
ceramic body B	+	+	+	+	+	+
dark green B5	+		+	+	+	
light green B3	+	+	+	+	+	+
yellow B1	+		+	+	+	
yellow B2	+		+	+	+	
blue B1	+		+	+	+	
blue B3	+		+	+	+	
dark blue B2	+		+	+	+	
white glaze and red/white polychromy B4	–		+	+	+	
dark brown B1	+		+	+	+	

Molecular analysis by way of micro-Raman spectroscopy (MRS) was performed on the cross-sections using the mapping mode for better observation of individual components presented in each of the glaze layers. The cross-sections were analysed using a micro-Raman spectrometer Nicolet DXR (Thermo Scientific, USA) in combination with an Olympus confocal microscope fitted with an objective 100 × and a CCD camera for signal detection. Two diode lasers with wavelengths 532 nm and 780 nm with output powers ranging between 1 and 10 mW or 5 and 20 mW, respectively, were used as the excitation sources. Calibration was performed using a polystyrene standard. The measurement took place within the range 50 – 3300 cm^{-1} with spectral resolution 4 cm^{-1}. The accumulation time ranged between 1 and 3 minutes. The spectra were evaluated by software Omnic 9.

The scanning electron microscopy and elemental analyses (SEM-EDS) were carried out using a scanning electron microscope with an energy dispersive X-ray analyser on the JEOL 6460 equipment with a Si (Li) X-ray detector. The analysis was conducted in low vacuum under pressure 35 Pa and acceleration voltage 20 kV using a backscattered electron detector. Mapping analysis of the element composition on the sections was carried out on the TESCAN MIRA3 RISE analysis unit equipped with an EDS analysis system Oxford EDS AZtec X-MAX80. The analysis was conducted in vacuum (70 Pa), acceleration voltage 20 kV, using BSE and SE detectors. The quantitative element mapping was performed using the analyser Oxford instruments AZtec software. Graphite coating was applied on the sample to create a polished cross-section.

The expansion measurements of ceramic body and green glaze were conducted using two thermal analysis techniques. The ceramic body of lunette A was measured by way of dilatometric measurements (Linseis L75 HS 1600C PT) in helium flow on approx. 20 mm-long compact samples with diameter 5 mm in the temperature range between 25 and 700 °C. The green glaze was measured using thermomechanical analysis (TMA CX04; R.M.I.) at a heating rate corresponding to the dilatometric measurements [5].

RESULTS AND DISCUSSION

Chemical and mineralogical composition of ceramic bodies and glazes in the lunettes

Chemical compositions of ceramic bodies and green glazes (A dark green, B3 light green) in both reliefs determined by XRF analysis are presented in Table 2 and Table 3, respectively. The similarities of dark green glazes were confirmed by SEM-EDS and by portable XRF analyses (Figure 4). The analyses showed mainly the presence of Si + Cu + Pb; i.e. the green colour of the glaze is mainly due to a copper ionic dye.

Mineralogical compositions obtained by evaluating the XRD patterns of ceramic bodies of the analysed fragments are shown in Figure 5. Mineralogical compositions of the samples were very similar, containing quartz as the main crystalline phase accompanied by a small amount of feldspars (mainly microcline), anatase, and traces of mullite and mica.

Raman spectroscopy confirmed the presence of both quartz (identification of the main peak ~466 cm^{-1}) and anatase (the signal at ~144 cm^{-1} associated with peaks at positions 396, 515 and 638 cm^{-1}). The measured spectra (Figure 6) showed that in addition to anatase, the samples contain another titanium dioxide modification – rutile (peaks at 143, 235, 445 and 613 cm^{-1}). Hematite with peaks at positions 226, 295, 411, 505 and 619 cm^{-1} was found as an additional admixture. Rutile, anatase and hematite grains are dispersed relatively irregularly within the ceramic body. The XRD analysis did not show the presence of rutile and hematite, likely because their amounts are below the detection limit of this method.

The XRF, XRD and SEM-EDS results showed that ceramic bodies and green glazes have very similar compositions. This proved that they were made in the same workshop, i.e. they were not made in two different workshops that shared the same mould.

Table 2. Chemical composition of ceramic bodies in wt. %.

	Na_2O	MgO	Al_2O_3	SiO_2	K_2O	CaO	TiO_2	Fe_2O_3	P_2O_5	V_2O_5	Cr_2O_5	MnO	ZrO_2	BaO	PbO
A	0.6	0.5	29	63	1.9	0.5	2.5	1.9	0.1	0.03	0.01	0.02	0.1	0.04	0.1
B	0.5	0.6	30	63	1.8	0.5	2.7	2	0.1	0.03	0.02	0.014	0.08	0.05	0.03

Table 3. Chemical composition of the ceramic green glazes in wt. %.

Green	Na_2O	MgO	Al_2O_3	SiO_2	K_2O	CaO	TiO_2	Fe_2O_3	PbO	P_2O_5	SO_3	Cl	V_2O_5	NiO	CuO	ZnO	As_2O_3	SeO_2	SnO_2	Sb_2O_3
A	0.2	0.1	5	55	0.4	1	0.3	0.3	35	0.2	0.1	0.1	0.02	0.1	2.5	0.01	0.1	0.01	0.1	0.1
B3 light	1	0.2	2	28	0	5	–	1	45	5	1	1	–	–	2	–	–	–	8	–

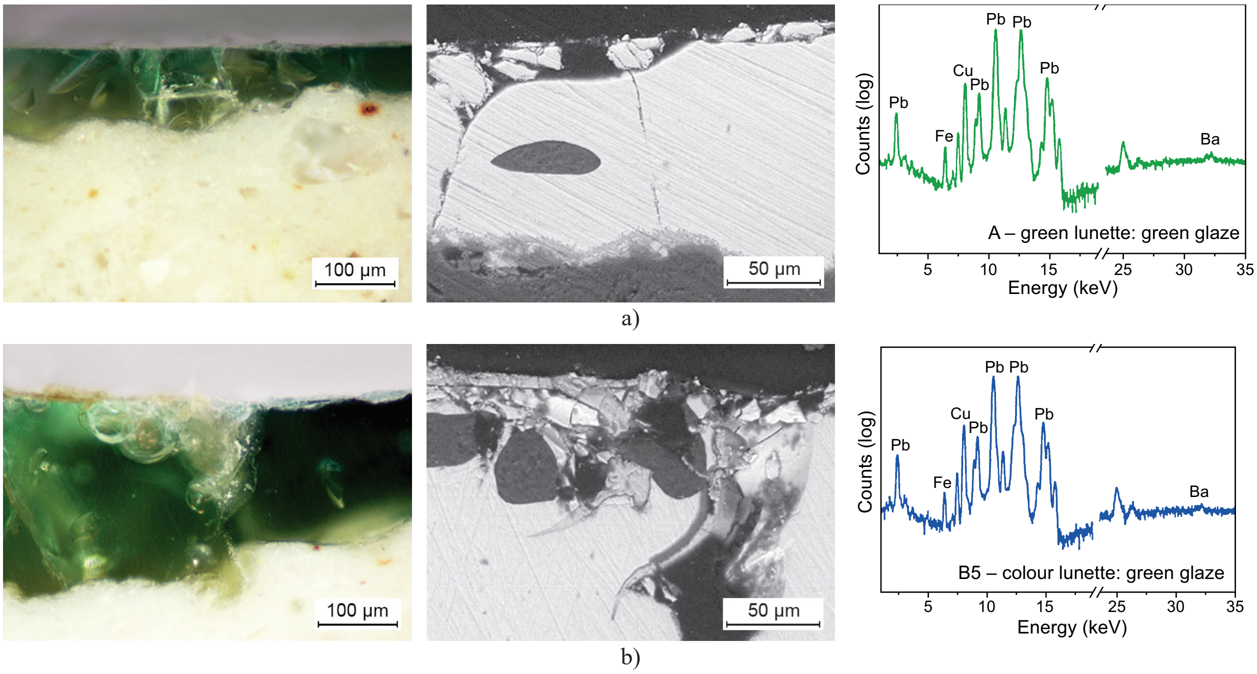

Figure 4. VIS and BSE cross-section of green glazes: a) green lunette, b) multi-colour lunette and XRF spectra.

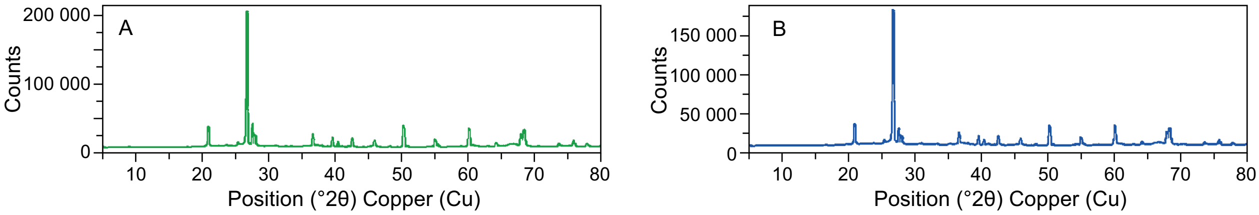

a) green lunette

b) multi-colour lunette

Figure 5. XRD pattern of ceramic bodies in both reliefs: a) green lunette, b) multi-colour lunette.

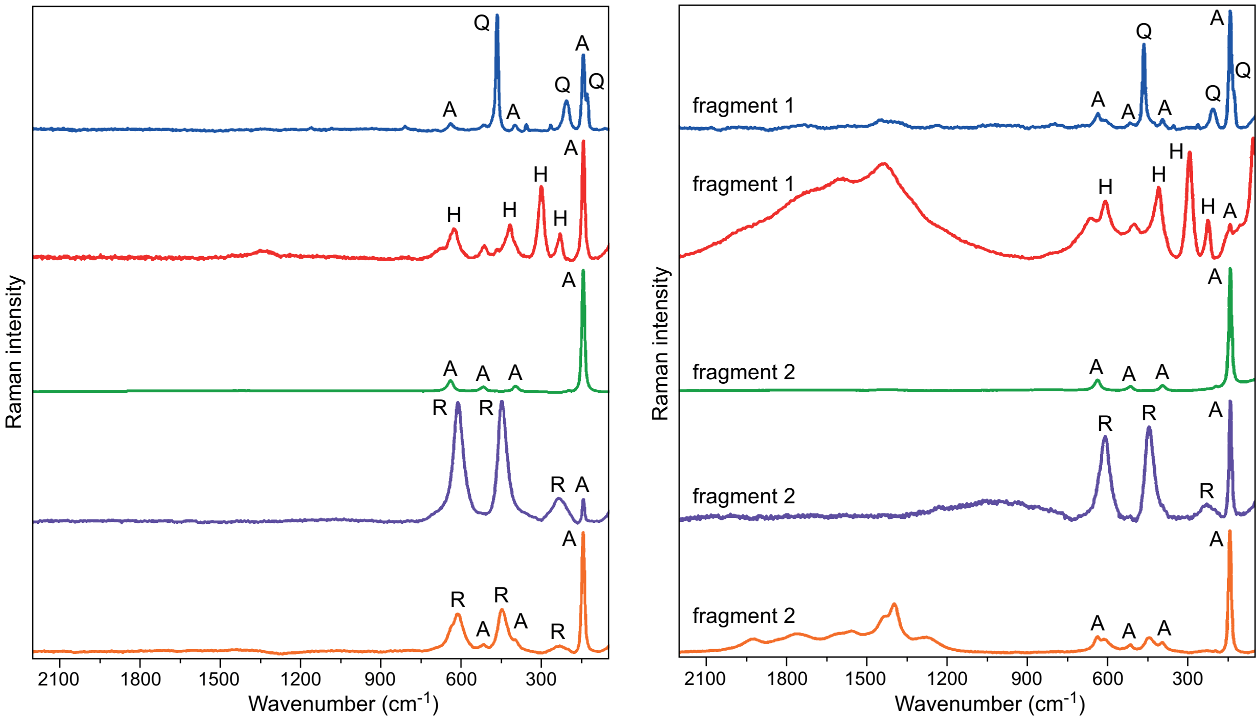

a) green lunette

b) multi-colour lunette

Figure 6. Raman spectra of minerals identified in the ceramics bodies: A – anatase, R – rutile, Q – quartz, H – hematite.

Table 4. Portable XRF results for the chemical composition of coloured glazes.

	Colour	Figure	Main component	Minor component
Green lunette	dark green A	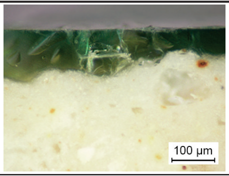	Si, Cu, Pb	Al, K, Ca, Ti, Fe, Ba, Sr
Multi-colour lunette	dark green B5	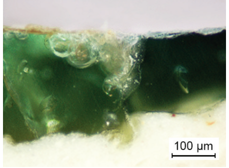	Si, Cu, Pb	Al, P, K, Ca, Ti, Fe, Ba, Sr
	light green B3	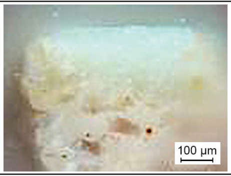	Si, Cu, Sn, Pb	Al, P, Ca, Fe, Ba, Ti, Sr, Zr
	yellow B1	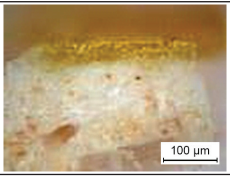	Si, Sn, Sb, Pb	Al, P, K, Ca, Fe, Ti, Ba, Zr
	yellow B2	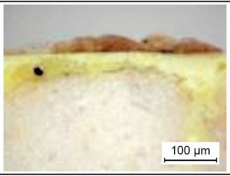	Si, Sn, Sb, Pb	P, K, Ca, Cu, Fe, Ti, Ba, Zr
	blue B1	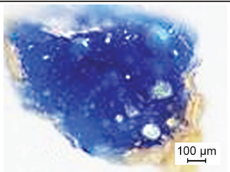	Si, Ca, Fe, Cu, Sn, Sb, Pb	Al, P, K, Ti, Ba, Sr, Zr
	blue B3	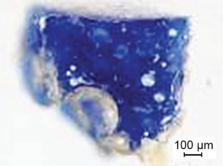	Si, Ca, Fe, Cu, Co, Sn, Pb	P, K, Ti, Ba, As, Sr, Zr
	dark blue B2	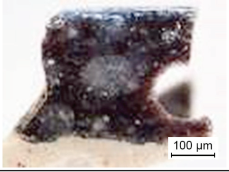	K, Si, Fe, Cu, Sn, Pb	Co, Ti, Ba, Sb, Sr, Zr
	dark brown B1	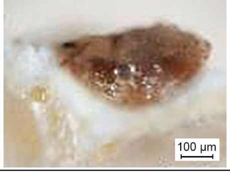	Si, P, Ca, Cu, Mn, Sn, Sb, Pb	Al, K, Ti, Ba, Sr, Zr
	white glaze B1 and white glaze with red/white polychromy B4	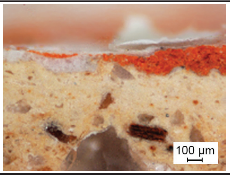	white glaze B1 Si, Ca, Sn, Pb	white glaze B1 Al, P, K, Ti, Fe, Sr, Zr

The chemical composition of the individual coloured glazes in both lunettes was determined by a combination of portable XRF (Table 4) and SEM-EDS (Table 5) on a cross-section from the spot or area of interest. The results showed that these are medium-lead glazes with a PbO content ranging between 28 and 63 wt. %. The low firing temperatures were due to the contents of PbO, the alkaline components K_2O and Na_2O and the relatively low amount of SiO_2. The dyeing components largely consisted of ionic dyes (Cu, Fe, Co, Sb, Mn ions).

Table 5. Semi-quantitative EDS results of chemical compositions of glazes (in wt. %).

	Color	Na_2O	MgO	Al_2O_3	SiO_2	P_2O_5	SO_3	Cl	K_2O	CaO	TiO_2	FeO	CoO	CuO	SnO_2	Sb_2O_3	PbO
Green lun.	dark greenA	0	0.06	5.19	35.51	0	0	0	0.26	0.33	0.63	0.39	0	2.65	0	0	54.98
Multi-colour lunette	dark green B5	0	0.12	3.45	33.87	0	0	0	0.20	0.37	0.34	0.27	0	2.83	0	0	58.56
	light green B3	1.68	0.13	1.57	34.70	0	0	0	0.50	0,14	0	0	0	1.87	9.71	0	49.71
	yellow B1 upper layer	0.07	0.13	6.11	34.11	0	0	0	0.17	0.66	0.42	2.23	0	0	8.36	6.37	41.36
	yellow B1 bottom layer	0.21	0	7.06	28.83	0	0	0	0.79	0.11	0.81	1.02	0	0	0.88	5.04	55.24
	yellow B2 upper layer	0.06	0.10	5.85	29.30	2.85	0.73	0	0.14	1.81	0.47	1.93	0	0	6.85	5.07	44.84
	yellow B2 bottom layer	0.21	0	5.76	28.34	0	0	0	0	0	0.66	1.04	0	0	0.70	0.71	62.60
	blue B1	5.73	0	2.73	53.42	0	0	0	7.34	1.06	0	0.74	0.54	0	0	0	28.46
	blue B3	5.21	0	2.40	53.59	0	0	7.70		0.82		0.39	0.46	0	0.69	0	28.83
	dark blue B2 upper layer blue	5.27	0.01	1.79	51.07	0	0	0	7.28	1.38	0	0.44	0	0.63	1.93	0	30.21
	white glaze (B4)	1.96	0.29	5.15	44.85	0	0	0	1.11	0	0	0.25	0	0	9.96	0	36.45

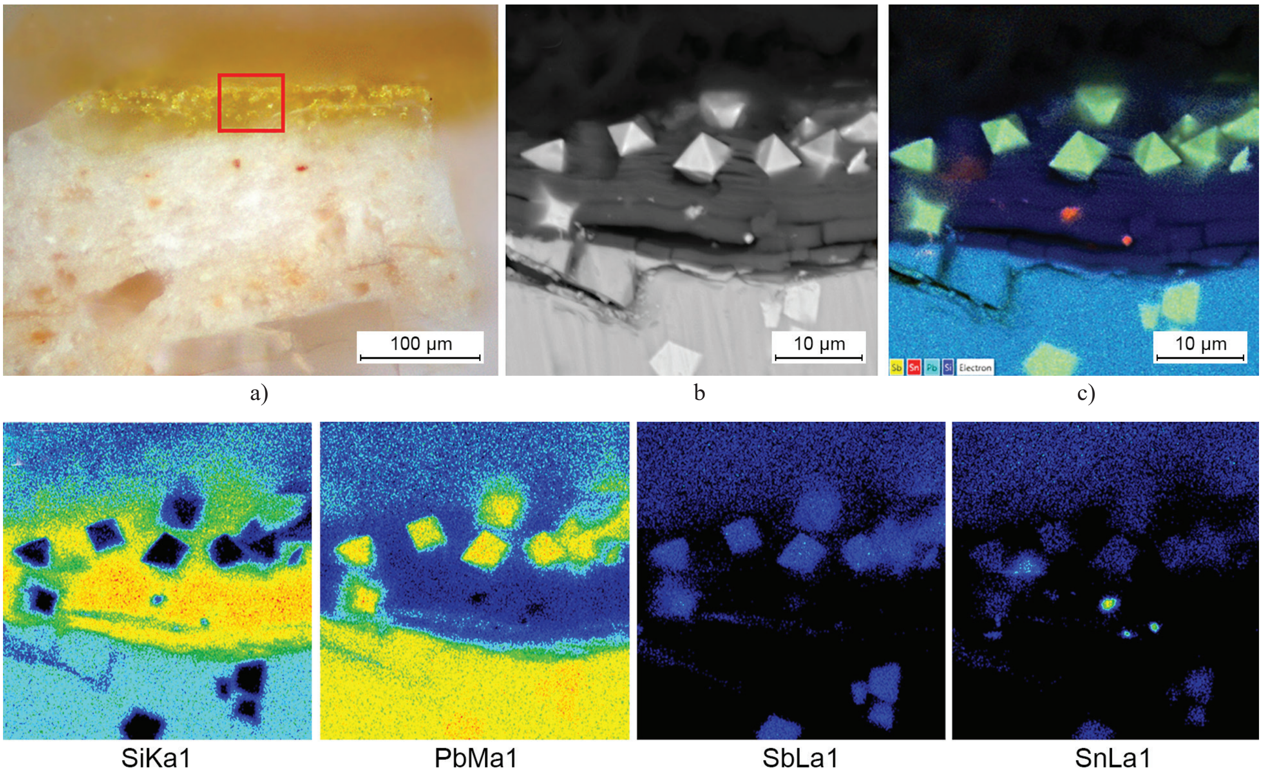

a) b c)

d)

Figure 7. Cross-section including the mapping area (a), BSE (b) and mapping images (c) of the yellow glaze (fragment B1) four corresponding individual qualitative and quantitative mapping images of Si, Pb, Sb and Sn, respectively (d).

EDS mapping was performed on the yellow-glaze sample fragment B1 (Figure 7). Figure 7 shows the qualitative distribution of lead, silicon, tin and antimony in the individual layers. The quantitative analysis of the distribution of dominant chemical elements showed a higher content of lead than that of silicon in the bottom layer and a minor presence of antimony and tin.

In the sample from the yellow glaze in fragment B2, a significantly higher amount of silicon was detected in the top layer of the glaze, while lead appears in localized particles which also contain antimony and tin. Peaks at ~ 69, 139, 336 a 504 cm^{-1} – the positions characteristic of the Naples yellow – were detected in the Raman spectra of these particles. A similar distribution of particles was observed in the bottom layer of the lead glaze with dominant presence of lead in the stratigraphy of the yellow glaze in fragment B1 (Figure 7). This layer appears semi-transparent. The second glaze layer with dominant presence of silicon contains cubic pyrochlore structure crystals. These crystals consist largely of lead and antimony combined. Raman spectroscopy of cubic pyrochlore crystals showed bands characteristic of Naples yellow (Pb-Sb). The main band corresponding to the Pb–O lattice vibration is variable, ranging between 138 and 145 cm^{-1} in a single crystal (Figure 8) [7-8]. The peak at ~504 cm^{-1} is related to SbO_6 structures and the peak at ~336 cm^{-1} corresponds to Sb–O and Pb–O bonds. The change in peak character at the antimony position within the grid may indicate that here antimony was substituted by tin. In the case of the bottom glaze layer, we obtained a spectrum in which a peak at ~ 450 cm^{-1} was observed in addition to the above-mentioned peaks. This peak at ~450 cm^{-1} is attributed to a tin modification [9] and was not identified in the spectra from the top glaze layer containing pyrochlore crystals. Spectra featuring a band at ~635 cm^{-1}, pertaining to the structure of cassiterite, were observed in some places. This corresponds with the distribution of lead and antimony in the top layer. The localized tin positions with lead and antimony absent from the structure suggest the presence of cassiterite SnO_2 in the top layer of the glaze. The obtained results also point to the possible presence of lead-tin

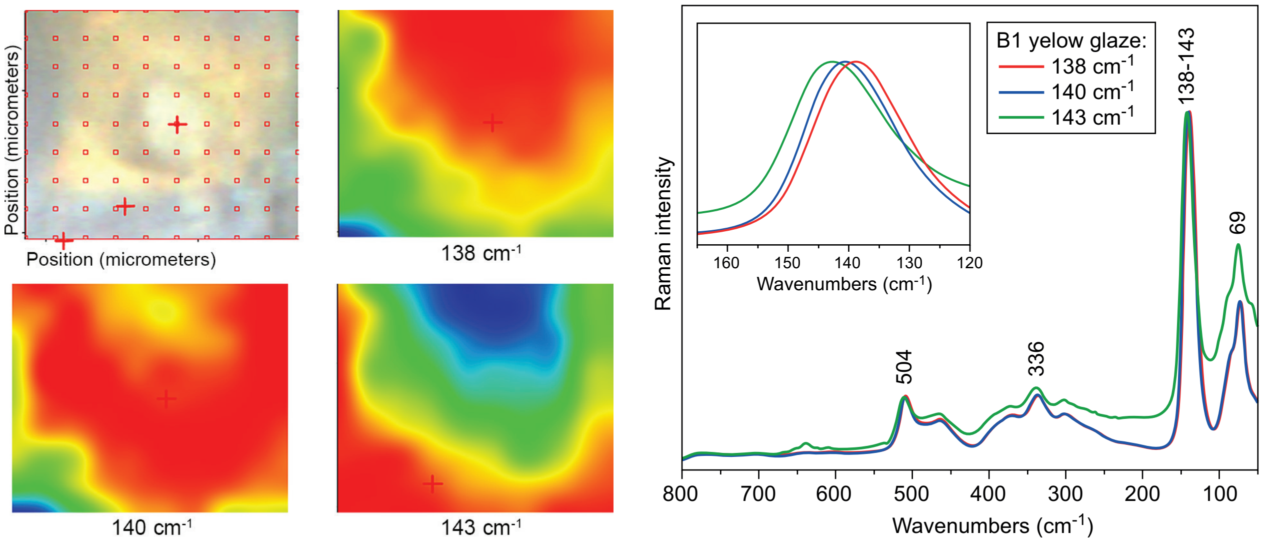

a) b)

Figure 8. Raman maps and spectra of the cubic pyrochlore crystal in the yellow glaze.

Table 6. Raman band wavenumbers of Naples yellow and lead-tin yellow type I and II (standards of Kremer Pigmente GmbH).

Pigment	No.	Chemical formula	Symmetry	Wavenumbers (cm^{-1}), laser 532 nm
Naples yellow, Paris (lead antimony tin oxide)	10130	$Pb(SbSn)O_3$	cubic pyrochlore	72m, 140vs, 335m, 464vw, 512m, 637vw, 723m
Naples yellow, dark (lead antimony tin oxide)	43125	$Pb_2Sb_2O_7$	cubic pyrochlore	77m, 148vs, 345m, 467w, 756w
Naples yellow, redish (lead antimony oxide)	43130	$Pb_3(SbO_4)_2$	cubic pyrochlore	75m, 145vs, 344m, 466w, 511w, 756w
Lead tin yellow type I (lead tin oxide)	10100	Pb_2SnO_4	orthorhombic	80m, 130vs, 196 m, 272sh, 290w, 379w, 454w, 525vw, 547vw
Lead tin yellow type II (lead tin silicon oxide)	10120	$Pb(SnSi)O_3$	cubic pyrochlore	67s, 138vs, 263 vw (sh), 325vw (sh), 450 sh, 635vw (sh)

yellow type II structure or Pb–Sb–Sn-based structure in the bottom glaze layer. The above-mentioned crystal structures may have formed because the raw materials were not homogeneous or due to the conditions during the firing process [10]. The term Naples yellow is used for Pb–Sb-based structural analogues but lead-tin yellow type II structure (lead-tin silicon oxide) may also occur after firing if tin is present (Table 6).

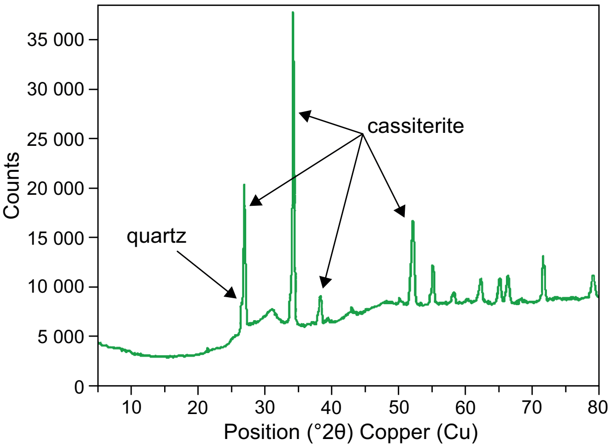

Figure 9. XRD spectra of light-green glazes B3.

Raman spectra with peaks 633 and 142 cm^{-1} were observed in the layer of light-green glaze. The 633 cm^{-1} peak corresponds to the lattice vibration Sn–O of cassiterite. XRD confirmed the presence of cassiterite (Figure 9). The colour of the light-green glaze depends on whether the copper-based ionic dye is present or not.

Secondary polychrome layers were identified in the sample from fragment B4 (Figure 10). The red polychrome layer on the white lead-tin glaze contains red lead and traces of lead white. Two layers of a white retouch were observed on this red polychrome layer. Calcium sulphate (gesso) was detected in the bottom layer of fragment B4 by way of Raman spectroscopy. Titanium white with rutile structure combined with phthalocyanine blue was found in the top layer of the fragment. We may assume the top coating was added after 1940.

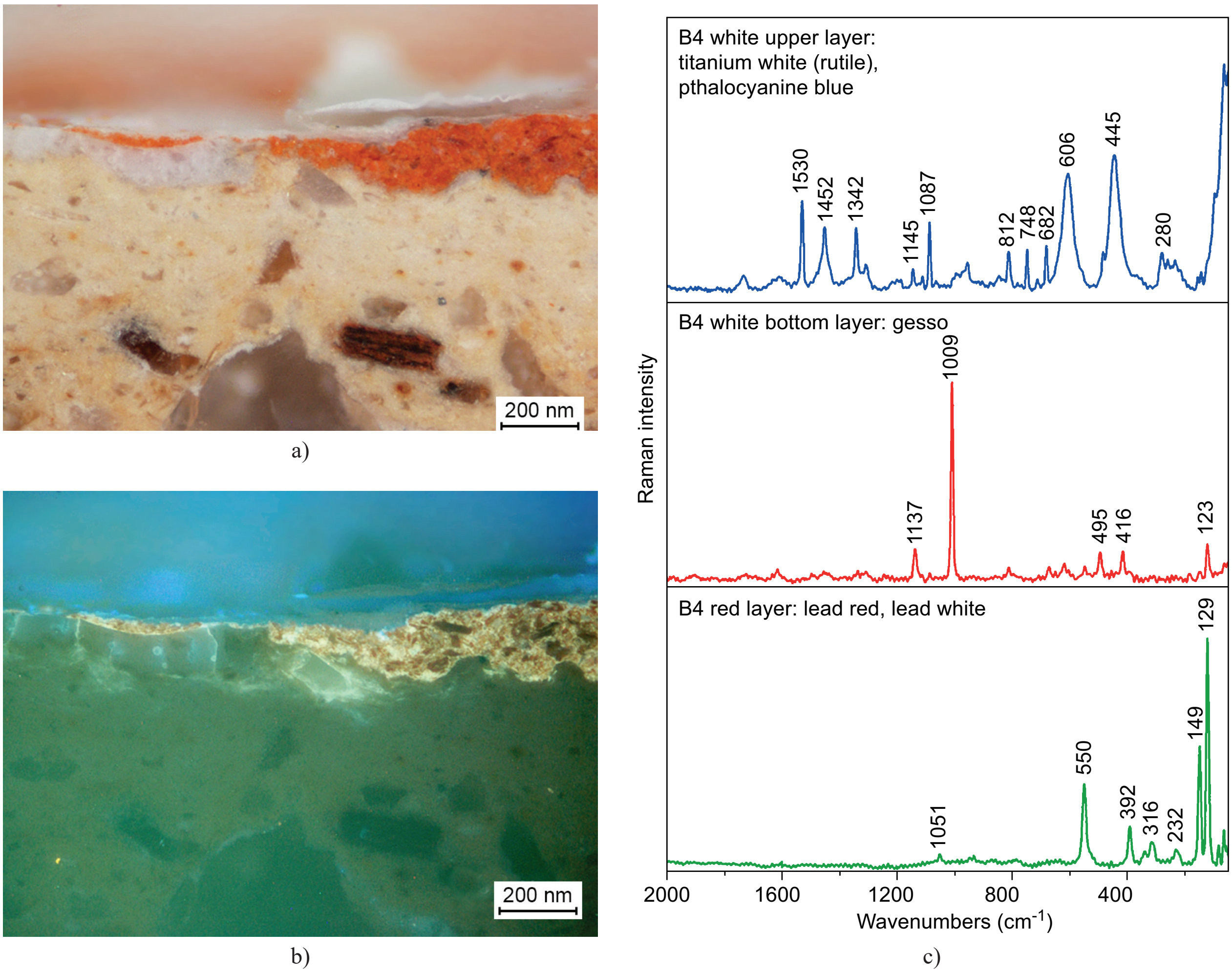

a)

b)

c)

Figure 10. The cross-section of the red and white polychrome on the top white glaze in visible (a) and ultraviolet light (b) and Raman spectra of the polychrome (c).

Identification of glaze defects and their causes

By finding out what caused the defects on the surface glaze layer, we gain invaluable knowledge about how archaeological glazed ceramic products were made and used. In order to confirm the possible source of defects, we used the relative expansion data obtained from dilatometric measurements to study stress relations in two-component systems [5-6, 11-1]. The stress relations between the green glazes and their ceramic substrates may have been influenced by higher amounts of unstable metaclays in the ceramic bodies. The graphic evaluations presented below show the actual stress relations in the systems. Matching the relative expansions in ceramic bodies and glazes (Figure 11) helps us observe the actual superposition of expansion traces. If the glaze curve (line) is below the ceramic-body curve (dashed line), tensile stress develops in the glaze. If the glaze curve is above the body curve, there is a compressive stress in the glaze layer, and ideal matching is achieved when the difference of the thermal expansion coefficients is not too large [5]. The green glazes in both reliefs are crazed, but the research has shown that crazing was caused by improper storage and irreversible moisture expansion in ceramic bodies. This type of glaze defects is referred to as delayed crazing. The results showed that the stress in the system changed as the ceramic body expanded due to moisture in the waste pit environment, reversing the compressive stress in the green glaze to tensile stress. These altered stress relations then caused corrosion.

The second dilatometric measurement showed the behaviour of the system immediately after firing. The measurements detected induced stress within the glaze which was in accordance with its ceramic substrate. The relative expansion curves from the first dilatometric measurement indicated a tensile stress in the glazes triggered by the irreversible moisture expansion in the ceramic bodies. However, the second measurement, which indicated the state of the system shortly after it had been fired, confirmed that there was in fact a compressive stress in the surface layer (Figure 11).

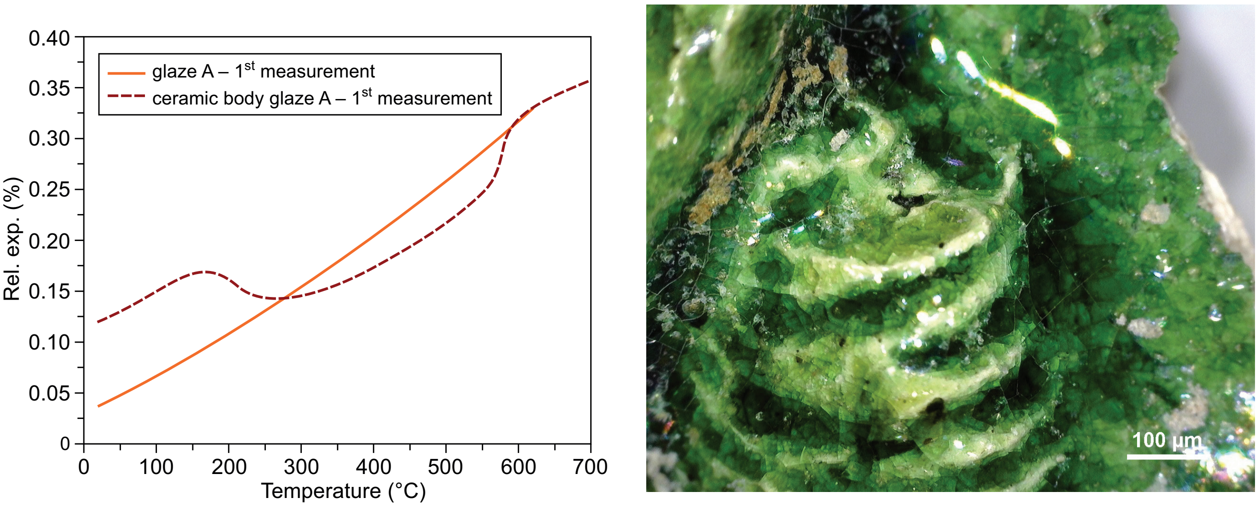

a)

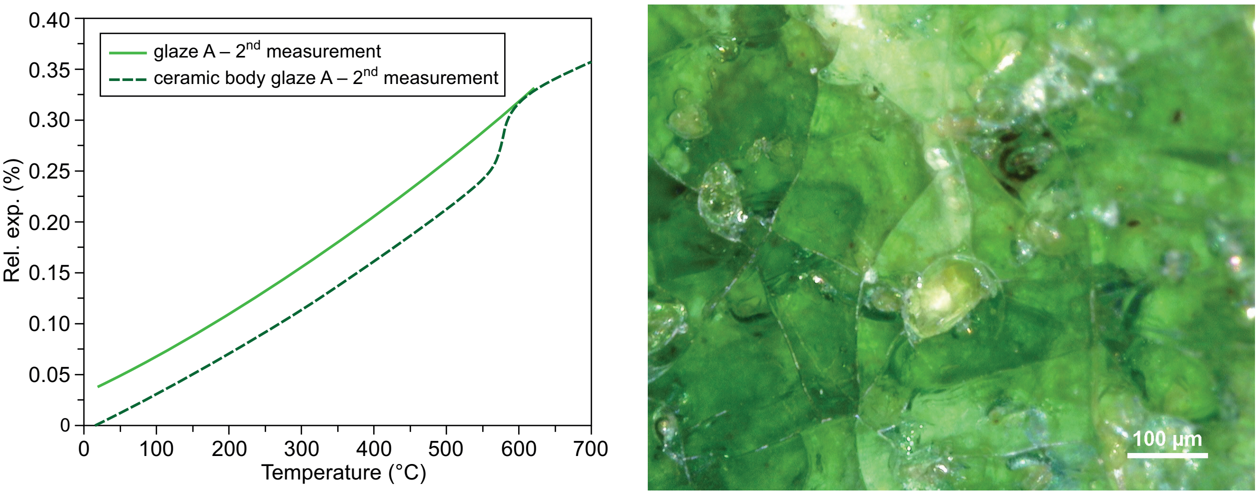

b)

Figure 11. Dilatometric measurements of ceramic body and green glaze (fragment A green lunette).

The corrosion of yellow glaze was caused by selective leaching of metal, largely lead cations from the glassy structure of the glaze (Figure 7). This selective leaching caused the formation of defects called pits or pinholes. The resulting leached surface layer then allowed for further corrosion. The incongruent corrosion of the surface layer was induced by improper environmental conditions in the waste pit.

CONCLUSION

The analyses proved that ceramic bodies and green glazes in both of the lunettes have very similar chemical compositions. We may therefore assume that the lunettes were made in the same workshop. Therefore, the multi-colour lunette could be used as a source to create the missing portion of the green relief.

The investigation into compositions of decorative layers showed that lead glazes with 28 – 63 wt. % PbO were coloured with ionic dyes (Cu, Fe, Co, Sb, Mn ions). Green glazes were coloured with a combination of Cu-Fe, with an addition of cassiterite creating a lighter green. A Co-component was found in the blue glazes. Using micro-Raman spectroscopy, the yellow pigments were identified as Naples yellow and lead-tin yellow structure type II or Pb-Sb-Sn. The central fragment with the lion was used to identify the secondary layers of polychrome (Figure 11). The red layer of polychrome consisted of red lead and two layers of white retouches – the first, bottom layer consisted of calcium sulphate (gesso) and the second layer contained titanium white with rutile structure combined with phthalocyanine blue. This top coating was added after 1940.

The investigation into causes and origins of glaze defects focused on degradation of green and yellow glazes. In the case of the yellow glaze, a higher content of lead component was detected by SEM-EDS mapping in the layer closer to the glaze–ceramic body interface. Conversely, more silica component and pigment components in the form of pyrochlore crystals were identified in the top layer of the glaze. The defect referred to as corrosion holes or pits was caused by selective leaching of lead component from the surface of the glaze due to corrosive environment in the waste pit. The green glazes were severely crazed due to moisture expansion in ceramic bodies inducing tensile stress within the glaze layer. The stress relations in the glaze–ceramic body systems were confirmed by the second dilatometric measurement of ceramic bodies, which showed the behaviour of the system immediately after firing. The second measurement and subsequent detection of induced stresses within both layers showed that both the glaze and its ceramic substrate were chosen correctly, creating a compatible, durable system.

Acknowledgements

This work was financed from the project of the Ministry of Culture Czech Republic: „Technology of Treatment and Identification of Degradation Processes of Ceramic Finds from Hradčany Palaces - Methods of Restoration and Conservation of Porous and Dense Ceramics and Porcelain"(DG18P02OVV028).

REFERENCES

1. Blažková G., Frolík, J. (2005): Architektura odhalená archeologickým výzkumem a problémy s její památkovou ochranou. Archaeologia historica, 30, 34–39.
2. Blažková G. (2006): Schwarzenberský palác, in: DRAGOUN, Z. a kol., Archeologický výzkum v Praze v letech 2003–2004. Pražský sborník historický. 34, 320–321.
3. Taylor J.R., Bull A.C. (1986). Ceramics Glaze Technology. 1st ed. Oxford: Pergamon Press. ISBN 0-08-033466-0.
4. Kloužková A., Kavanová M., Kohoutková M., Klápšťová K., Dvořáková P., Michalcová A. (2018): Archaeometric study of ancient Maya figurines from the collection of the National Museum. Ceramics – Silikaty, 6(4), 418-431. doi: 10.13168/cs.2018.0036
5. Kavanová M., Kloužková A., Kloužek J. (2017): Characterization of the interaction between glazes and ceramic bodies. Ceramics – Silikaty, 61(3), 267-275. doi: 10.13168/cs.2017.0025.
6. Özçatal M., et al. (2014): Characterization of lead glazed potteries from Smyrna (Izmir/Turkey) using multiple analytical techniques; Part I: Glaze and engobe. Ceramics International, 40, 2143-2151. doi: 10.1016/j.ceramint.2013.09.014
7. Sandalinas C., Ruiz-Moreno S., Lopez-Gil A., Miralles J. (2006): Experimental confirmation by Raman spectroscopy of a Pb-Sn-Sb triple oxide yellow pigment in sixteenth-century Italian pottery. Journal of Raman Spectroscopy, 37, 1146-1153. doi: 10.1002/jrs.1580
8. Kırmızı B., et al. (2010): On-site analysis of Chinese Cloisonné enamels from fifteenth to nineteenth centuries. Journal of Raman Spectroscopy, 41(7), 780-790. doi: 10.1002/jrs.2516
9. Rosi F., et al. (2011): Raman scattering features of lead pyroantimonate compounds: implication for the non-invasive identification of yellow pigments on ancient ceramics. Part II. In situ characterisation of Renaissance plates by portable micro-Raman and XRF studies. Journal of Raman Spectroscopy, 42(3), 407-414. doi: 10.1002/jrs.2699
10. Sakellariou K., Miliani C., Morresi A., Ombelli M. (2004): Spectroscopic investigation of yellow majolica glazes. Journal of Raman Spectroscopy, 35, 0377-0486. doi: 10.1002/jrs.1084
10. Kloužková A., Kavanová M., Kohoutková M., Zemenová P., Dragoun Z. (2016): Identification of causes of degradation of Gothic ceramic tiles by thermal analyses. Journal of Thermal Analysis and Calorimetry, 125(3),1311-1318. doi: 10.1007/s10973-016-5488-5
11. Plešingerová B., Klapáč M., Kovalčíková M. (2002): Moisture expansion of porous biscuit bodies – reason of glaze cracking. Ceramics – Silikaty, 46(4), 159-165.